Observation of coherent population transfer in a four-level tripod system with a rare-earth-metal-ion-doped crystal

Hayato Goto and Kouichi Ichimura
Frontier Research Laboratory, Corporate Research and Development Center, Toshiba Corporation, 1, Komukai Toshiba-cho, Saiwai-ku, Kawasaki-shi, 212-8582, Japan

(Received 11 October 2006; revised manuscript received 9 January 2007; published 15 March 2007)

Coherent population transfer in a laser-driven four-level system in a tripod configuration is experimentally investigated with a rare-earth-metal-ion-doped crystal ($Pr^{3+}:Y_2SiO_5$). The population transfers observed here indicate that a main process inducing them is not optical pumping, which is an incoherent process inducing population transfer. Moreover, numerical simulation, which well reproduces the experimental results, also shows that the process inducing the observed population transfers is similar to stimulated Raman adiabatic passage (STIRAP) in the sense that this process possesses characteristic features of STIRAP.

DOI: 10.1103/PhysRevA.75.033404 PACS number(s): 32.80.Qk, 03.67.Lx

I. INTRODUCTION

When a quantum system is initially in an eigenstate of the Hamiltonian whose variation is sufficiently slow, the system adiabatically follows the time-varying eigenstate. This process is called adiabatic passage, which is based on adiabatic approximation [1,2]. Since the adiabatic passage is a good technique to manipulate quantum states, a number of implementations of quantum computation based on adiabatic passage have been proposed [3–9]. A laser-driven three-level system in a Λ configuration provides a typical example of adiabatic passage. This system has a zero-eigenvalue eigenstate of the Hamiltonian. This eigenstate is called a dark state or a trapped state [10,11]. If the system is initially in the dark state and the variations of the laser fields are sufficiently slow, the system adiabatically follows the dark state. This adiabatic passage is called stimulated Raman adiabatic passage (STIRAP) [11]. The Λ STIRAP technique is a powerful tool for coherent and complete population transfer between two quantum states. Extensive theoretical investigations [12–23] and experimental demonstrations [24–30] of the population transfer via STIRAP have been reported. More recently, the STIRAP process in a four-level system in a tripod configuration has been studied theoretically [31–35] and experimentally [36,37]. The tripod STIRAP has some characteristics which the Λ STIRAP does not possess. For example, single-qubit rotations based on STIRAP are realized by the tripod STIRAP technique [4,6], but cannot be achieved by the Λ STIRAP one. One of the most interesting characteristics of the tripod STIRAP process is the appearance of non-Abelian geometric phases [4,32,33]. It is well known that quantum adiabatic evolutions are accompanied by geometric phase factors [38]. Berry first found that the geometrical phase factor appears, in addition to a dynamical phase factor, in an adiabatic quantum evolution with a nondegenerate eigenstate of a Hamiltonian [39,40]. The Berry phase was generalized to the case of a degenerate eigenspace of a Hamiltonian by Wilczek and Zee (WZ) [41]. Since the WZ geometric phase factors are expressed as matrices, they are in general noncommutable with one another and, therefore, are called non-Abelian. Since the tripod system has two degenerate dark states, the WZ geometric phases appear in the tripod STIRAP processes [4,32]. The geometric phases are also useful to control quantum states. Many proposals for quantum computation based on geometric phases have been reported [4,42–50].

In this paper, we report experimental investigation of the four-level tripod system in terms of STIRAP. Our experiment is performed with a rare-earth-metal-ion-doped crystal. Rare-earth-metal-ion-doped crystals, such as $Pr^{3+}:Y_2SiO_5$ (hereafter Pr:YSO) used here, have good characteristics, such as long coherence times of optical [51–55] and hyperfine [56–58] transitions, and optical controllability of the ionic states. Because of them, several implementations of quantum computation with these crystals have been proposed [5,59–64]. So far, electromagnetically induced transparency [56,65–67], light storage [68,69], and coherent state manipulation including quantum gate operations [48,70–72] have been realized with these crystals. Very recently, efficient population transfer by the Λ STIRAP technique has also been demonstrated with Pr:YSO [30]. However, the population transfer via tripod STIRAP has not been experimentally studied with these crystals, even with any solid material. Although a tripod system in Pr:YSO has been studied for optical switch [73,74], population transfer has not been investigated. In the present work, we perform several types of experiments of population transfer in the tripod system with a Pr:YSO crystal. By comparing the experimental results with one another and by using numerical simulation, we discuss whether or not the process inducing the observed population transfers is a coherent process, especially the STIRAP process.

This paper is organized as follows. In Sec. II, basic theory for the tripod STIRAP is explained. In Sec. III, the experimental setup and methods are described. In Sec. IV, experimental results are presented. In Sec. V, we discuss the experimental results. Numerical simulation is utilized for the discussion. The conclusion is presented in Sec. VI.

II. THEORY FOR TRIPOD STIRAP

Here we present a basic theory for coherent population transfer via tripod STIRAP. A four-level system in a tripod

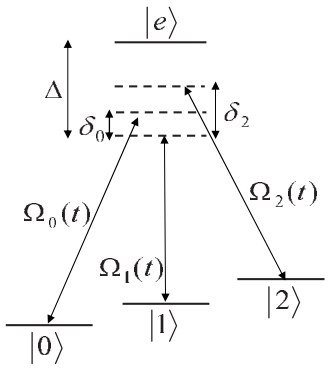

FIG. 1. Four-level system in a tripod configuration. Δ is the one-photon detuning from the $|1\rangle$-$|e\rangle$ transition. δ_0 and δ_2 are the two-photon detunings from the $|0\rangle$-$|1\rangle$ and $|1\rangle$-$|2\rangle$ transitions, respectively. $\Omega_j(t)$ $(j=0,1,2)$ is the Rabi frequency corresponding to the $|j\rangle$-$|e\rangle$ transition.

configuration interacting with three laser fields is depicted in Fig. 1.

The Hamiltonian in the rotating-wave approximation is given by

$$H(t) = \hbar\,\delta_0|0\rangle\langle 0| + \hbar\,\delta_2|2\rangle\langle 2| + \hbar\,\Delta|e\rangle\langle e| + i\frac{\hbar}{2}\sum_{j=0}^{2}\Omega_j(t)(|e\rangle\langle j| - |j\rangle\langle e|), \tag{1}$$

where Δ is the one-photon detuning from the $|1\rangle$-$|e\rangle$ transition, δ_j $(j=0,2)$ is the two-photon detuning from the $|j\rangle$-$|1\rangle$ transition, and $\Omega_j(t)$ $(j=0,1,2)$ is the Rabi frequency corresponding to the $|j\rangle$-$|e\rangle$ transition (the Rabi frequencies have been assumed to be real).

In this paper, we assume that the initial state is $|0\rangle$ and the Rabi frequencies for tripod STIRAP are set as

$$\Omega_0(t) = \Omega_0^{(0)} e^{-(t-t_0)^2/T_0^2}, \tag{2}$$

$$\Omega_1(t) = \Omega_1^{(0)} e^{-(t-t_1)^2/T_1^2}, \tag{3}$$

$$\Omega_2(t) = \Omega_2^{(0)}, \tag{4}$$

where $\Omega_j^{(0)}$ $(j=0,1,2)$ are positive constants, t_0 and t_1 denote the times at which $\Omega_0(t)$ and $\Omega_1(t)$ reach their maximum values, respectively, and T_0 and T_1 denote the pulse widths. This type of tripod STIRAP processes have been theoretically studied in Ref. [32]. In this section, we explain the ideal case where there are no decoherences and no detunings $(\Delta=\delta_0=\delta_2=0)$ [4,32].

There are two degenerate dark states expressed as

$$|D_0(t)\rangle = \sin\theta(t)|0\rangle - \cos\theta(t)\sin\phi(t)|1\rangle - \cos\theta(t)\cos\phi(t)|2\rangle, \tag{5}$$

$$|D_1(t)\rangle = \cos\phi(t)|1\rangle - \sin\phi(t)|2\rangle, \tag{6}$$

with

$$\tan\phi = \Omega_1/\Omega_2, \tag{7}$$

$$\tan\theta = \frac{\sqrt{\Omega_1^2+\Omega_2^2}}{\Omega_0}. \tag{8}$$

The initial and final dark states in the present case are as follows: $|D_0(-\infty)\rangle=|D_0(\infty)\rangle=|0\rangle$ and $|D_1(-\infty)\rangle=|D_1(\infty)\rangle=|1\rangle$. The other eigenvalues of the Hamiltonian are $\pm\hbar\sqrt{\Omega_0^2+\Omega_1^2+\Omega_2^2}/2$, and the corresponding eigenstates are given by

$$|B_\pm(t)\rangle = \frac{\cos\theta(t)|0\rangle + \sin\theta(t)\sin\phi(t)|1\rangle + \sin\theta(t)\cos\phi(t)|2\rangle \pm i|e\rangle}{\sqrt{2}}. \tag{9}$$

The so-called adiabatic condition is given by [2,75]

$$|\langle B_\pm|\dot{D}_0\rangle| = \left|\frac{\dot{\theta}}{\sqrt{2}}\right| \ll \frac{\sqrt{\Omega_0^2+\Omega_1^2+\Omega_2^2}}{2}, \tag{10}$$

$$|\langle B_\pm|\dot{D}_1\rangle| = \left|\frac{\dot{\phi}\sin\theta}{\sqrt{2}}\right| \ll \frac{\sqrt{\Omega_0^2+\Omega_1^2+\Omega_2^2}}{2}, \tag{11}$$

where the dot denotes time derivative. In the present case, this condition is satisfied if $T_0 \gg \Omega_2^{(0)-1}$ and $T_1 \gg \Omega_2^{(0)-1}$. When the adiabatic condition is satisfied, the state is approximately the superposition of only the two dark states, and expressed as follows:

$$|\psi(t)\rangle \simeq \alpha_0(t)|D_0(t) + \alpha_1(t)|D_1(t). \tag{12}$$

By inserting Eq. (12) into the Schrödinger equation, $i\hbar|\dot{\psi}\rangle = H|\psi\rangle$, we obtain

$$\frac{d}{dt}\begin{pmatrix}\alpha_0\\ \alpha_1\end{pmatrix} = -\begin{pmatrix}\langle D_0|\dot{D}_0\rangle & \langle D_0|\dot{D}_1\rangle\\ \langle D_1|\dot{D}_0\rangle & \langle D_1|\dot{D}_1\rangle\end{pmatrix}\begin{pmatrix}\alpha_0\\ \alpha_1\end{pmatrix} \tag{13}$$

and

$$\begin{pmatrix}\alpha_0(\infty)\\ \alpha_1(\infty)\end{pmatrix} = \begin{pmatrix}\cos\Theta & \sin\Theta\\ -\sin\Theta & \cos\Theta\end{pmatrix}\begin{pmatrix}\alpha_0(-\infty)\\ \alpha_1(-\infty)\end{pmatrix}, \tag{14}$$

where

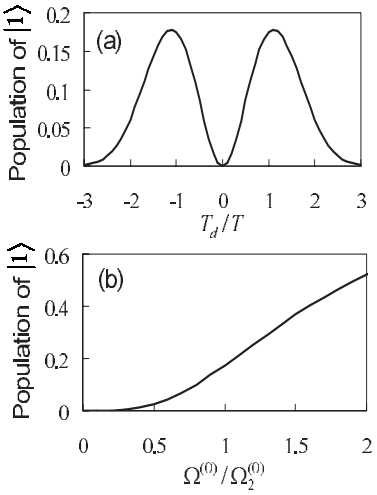

FIG. 2. Parameter dependence of the final population of $|1\rangle$ in the ideal tripod STIRAP processes. The Rabi frequencies are set as Eqs. (2)–(4). (a) Delay-time dependence. T_d denotes the delay time of the pulse sequence ($T_d \equiv t_0 - t_1$). T denotes the pulse width ($T \equiv T_0 = T_1$). The Rabi frequencies are set as $\Omega_0^{(0)} = \Omega_1^{(0)} = \Omega_2^{(0)}$. (b) Dependence on the peak Rabi frequency, $\Omega^{(0)} \equiv \Omega_0^{(0)} = \Omega_1^{(0)}$, of the two pulses. T_d is set to T ($T \equiv T_0 = T_1$).

$$\Theta = -\int \dot{\phi} \cos\theta \, dt = \int \sin\theta \, d\theta \, d\phi. \tag{15}$$

Θ is the solid angle swept by the vector pointing to the (θ, ϕ) direction. The rotation matrix in the right-hand side of Eq. (14) is an example of the WZ geometric phase factor [4,32,41]. The final state is given by

$$|\psi(\infty)\rangle \simeq \alpha_0(\infty)|D_0(\infty)\rangle + \alpha_1(\infty)|D_1(\infty)\rangle$$
$$= \cos\Theta|0\rangle - \sin\Theta|1\rangle, \tag{16}$$

where we have used $\alpha_0(-\infty)=1$, $\alpha_1(-\infty)=0$, $|D_0(\infty)\rangle = |0\rangle$, $|D_1(\infty)\rangle = |1\rangle$, and Eq. (14). Thus it turns out that the tripod STIRAP process in the present case induces the superposition of $|0\rangle$ and $|1\rangle$ from the initial state $|0\rangle$, and the final amplitudes are determined by the geometric phase.

Figure 2 shows how the final population of $|1\rangle$ in the ideal case, which is equal to $\sin^2\Theta$ from Eq. (16), depends on some parameters. These have been calculated numerically with Eqs. (7), (8), and (15). Figure 2(a) shows the dependence of the final population of $|1\rangle$ on the delay time, $T_d \equiv t_0 - t_1$, of the pulse sequence. T denotes the pulse width ($T \equiv T_0 = T_1$). The Rabi frequencies are set as $\Omega_0^{(0)} = \Omega_1^{(0)} = \Omega_2^{(0)}$. The population around $T_d = 0$ is smaller than those around $T_d = \pm T$ [32]. Figure 2(b) shows the dependence of the final population of $|1\rangle$ on the peak Rabi frequency, $\Omega^{(0)} \equiv \Omega_0^{(0)} = \Omega_1^{(0)}$, of the two pulses. T_d is set to T ($T \equiv T_0 = T_1$). The population increases monotonically with respect to $\Omega^{(0)}$. These properties of the tripod STIRAP process are discussed in Sec. V with the experimental results.

The relation between tripod STIRAP and single-qubit rotations is as follows [4]. Equation (14) holds for arbitrary initial states. This means that the WZ geometric phase factor [the rotation matrix in the right-hand side of Eq. (14)] can be directly applied to single-qubit rotations. In contrast, Λ STIRAP requires a pulse sequence depending on a initial state [11]. To achieve coherent population transfer from $|0\rangle$ to $|1\rangle$ by Λ STIRAP, it is necessary to use two partially overlapped laser pulses in the *counterintuitive* order in which a pulse initially couples the two empty states, $|1\rangle$ and $|e\rangle$, and next another pulse couples $|0\rangle$ and $|e\rangle$. If the order of the pulses is opposite, which is called the "intuitive" order, Λ STIRAP does not occur, and instead optical pumping, which is an incoherent process, occurs. In the case of tripod STIRAP, coherent population transfer can be achieved even in the case of the intuitive order, because of the presence of the third field coupling $|2\rangle$ to $|e\rangle$. This is a significant feature of tripod STIRAP.

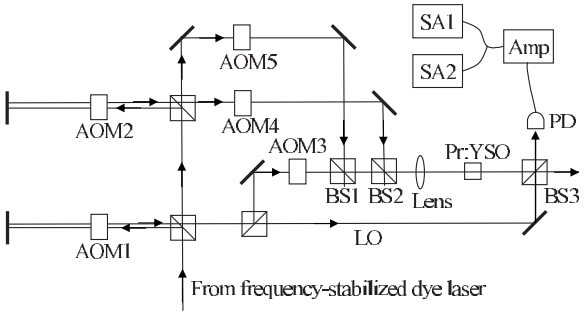

FIG. 3. Schematic of the experimental setup. AOM, acousto-optic modulator. BS, beam splitter. PD, photodiode. Amp, amplifier. SA, spectrum analyzer. LO, local oscillator.

III. EXPERIMENT

A. Experimental setup

The experimental setup is shown in Fig. 3. This is exactly the same as that used in Ref. [30]. The differences between the present experiment and Ref. [30] are only in laser frequencies and waveforms.

The light source is a ring dye (Rhodamine 6G) laser (Coherent 699-29) pumped by an argon ion laser (Coherent INNOVA400). The frequency jitter is reduced to several kHz over 15 ms by locking to the resonance frequency of an external stable cavity using the Pound-Drever-Hall method [76]. The frequency-stabilized laser is split into three beams. The frequencies of the three fields are set to ν_0, $\nu_1 = \nu_0 + 10.2$ MHz and $\nu_2 = \nu_0 + 27.5$ MHz ($\nu_0 \sim 494.72$ THz; see Fig. 5) by two acousto-optic modulators (AOM1 and AOM2 in Fig. 3). The waveforms of the three beams are controlled with the other three AOMs. The three beams are combined with two beam splitters (BS1 and BS2 in Fig. 3). The combined beam is tightly focused on the sample in a cryostat with a 100-mm-focal-length lens. The beam radius (e^{-2} in intensity) on the sample is about 16 μm. The sample is a 3-mm-thick Pr:YSO crystal whose Pr^{3+} concentration is about 0.05 at. %. The b axis is parallel to the direction of the beam. The polarization of the field is adjusted to obtain maximum absorption. The sample is kept at 4 K. The transmitted light interferes with a local oscillator and the transmission intensity is measured by heterodyne detection. The output of the photodiode is amplified by a wideband ampli-

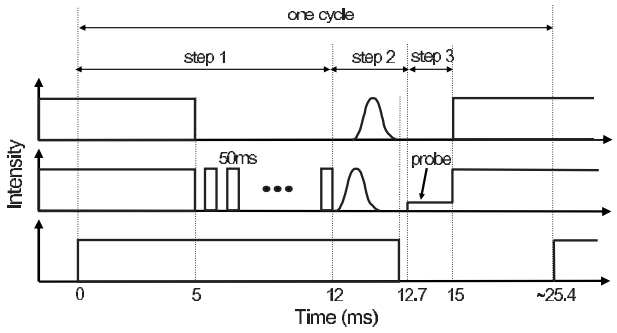

FIG. 4. Wave forms of the three fields used in the experiment. The top, middle, and bottom diagrams correspond to the fields of frequencies ν_0, ν_1, and ν_2, respectively. In step 2, the waveforms are set so that the Rabi frequencies given by Eqs. (2)–(4) are obtained (see Fig. 6 for details).

fier and input to two spectrum analyzers (SAs). The resolution and video bandwidths of the SAs are set to 1 MHz. The outputs of the SAs are input to a digital oscilloscope. All the data are accumulated over 64 cycles by the oscilloscope. The duration of one cycle is about 25 ms (see Fig. 4).

B. Wave forms of the three laser fields

As mentioned above, we use three laser fields of frequencies ν_0, ν_1, and ν_2. The waveforms of the fields are shown in Fig. 4. As shown in Fig. 4, the experimental procedure consists of the following three steps: Step 1 is appropriate preparation of the ionic state, including initialization of the ionic state to $|0\rangle$, by optical pumping with the three fields; step 2 is population transfer from $|0\rangle$ to $|1\rangle$ with a constant field of frequency ν_2 and two Gaussian pulses of frequencies ν_0 and ν_1; step 3 is the measurement of the final population of $|1\rangle$ with a weak probe field of ν_1. The details of these steps are described in the following.

C. Step 1: Initialization of ionic state

The energy-level diagram of Pr^{3+} ions doped in a YSO crystal is shown in Fig. 5 [77]. We use the $^3H_4$-$^1D_2$ transition of site-I Pr^{3+} ions in YSO. As shown in Fig. 5, $|^3H_4, \pm 1/2\rangle$, $|^3H_4, \pm 3/2\rangle$, and $|^3H_4, \pm 5/2\rangle$ are regarded as $|0\rangle$, $|1\rangle$, and $|2\rangle$, respectively, in Fig. 1. Since the Pr^{3+} ions have three

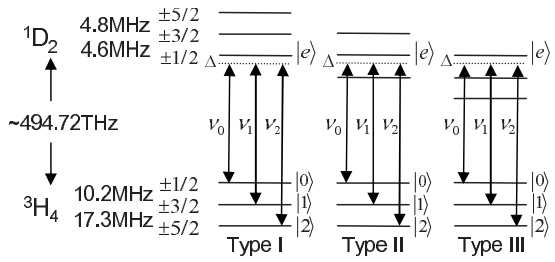

FIG. 5. Energy-level diagram of Pr^{3+} ions doped in a YSO crystal. Δ denotes one-photon detuning. Two-photon detunings are ignored (not shown). $|^1D_2, \pm 1/2\rangle$, $|^1D_2, \pm 3/2\rangle$, and $|^1D_2, \pm 5/2\rangle$ correspond to $|e\rangle$ in Fig. 1 for type-I, type-II, and type-III ions, respectively.

TABLE I. Estimated maximum Rabi frequencies, $\Omega_j^{(0)}/2\pi$ ($j=0,1,2$), in the case of Fig. 6(b). Rows and columns correspond to the ground and excited hyperfine levels, respectively. In other words, rows and columns correspond to $\Omega_j^{(0)}/2\pi$ and the ionic type (I, II, III), respectively.

$g\backslash e$	±1/2 (I)	±3/2 (II)	±5/2 (III)
±1/2 ($\Omega_0^{(0)}/2\pi$)	94	78	30
±3/2 ($\Omega_1^{(0)}/2\pi$)	80	98	10
±5/2 ($\Omega_2^{(0)}/2\pi$)	90	60	390

excited-state hyperfine levels and the optical transition is inhomogeneously broadened (~10 GHz [78,79]), there are three types of ions having a tripod configuration, as shown in Fig. 5. $|^1D_2, \pm 1/2\rangle$, $|^1D_2, \pm 3/2\rangle$, and $|^1D_2, \pm 5/2\rangle$ correspond to $|e\rangle$ in Fig. 1 for type-I, type-II, and type-III ions, respectively. We treat the three types of ions simultaneously.

Because of the inhomogeneous broadening of the optical transitions, there are many unnecessary ions which do not have a tripod configuration but have at least a transition interacting with a field. These unnecessary ions can be removed by optical pumping with the three fields. The role of the part from $t=0$ to 5 ms in step 1 in Fig. 4 is this pumping. By the pumping, the population of the unnecessary ions is concentrated on the ground states decoupled from any excited states. The other part of step 1 concentrates the population of the ions used for the experiment on $|0\rangle$ by optical pumping. In this interval, the field of ν_1 is applied as square pulse sequence so that coherent population trapping does not prevent the pumping.

By the method explained here, we can initialize appropriately the ions with the transitions whose one-photon detunings from the corresponding laser fields are smaller than the corresponding Rabi frequencies (~100 kHz; see Table I). In this way, we do not prepare the ensemble of ions with a narrow inhomogeneous linewidth, as performed in Refs. [72,77]. Instead, we estimate the population of the ions with a specific value of the one-photon detuning, Δ, by the measurement method explained in Sec. III E.

D. Step 2: Population transfer

After the preparation and initialization of the ionic state, the intensities of the fields are controlled so that the Rabi frequencies given by Eqs. (2)–(4) are obtained (see Fig. 6 for details). The pulse widths, T_0 and T_1, are set to 100 μs in the present experiment.

E. Step 3: Measurement of population

In step 3, a weak probe field of frequency ν_1 is injected to estimate the final population of $|1\rangle$ (see Fig. 4). The intensity of the probe is about 1/100 of the maximum intensity of the field of ν_1. The transmission intensities are measured by heterodyne detection. In Ref. [30], we have described in detail how the population is estimated from the measured transmittance of the probe. While a single transition interacts with a probe in the case of Ref. [30], three transitions having dif-

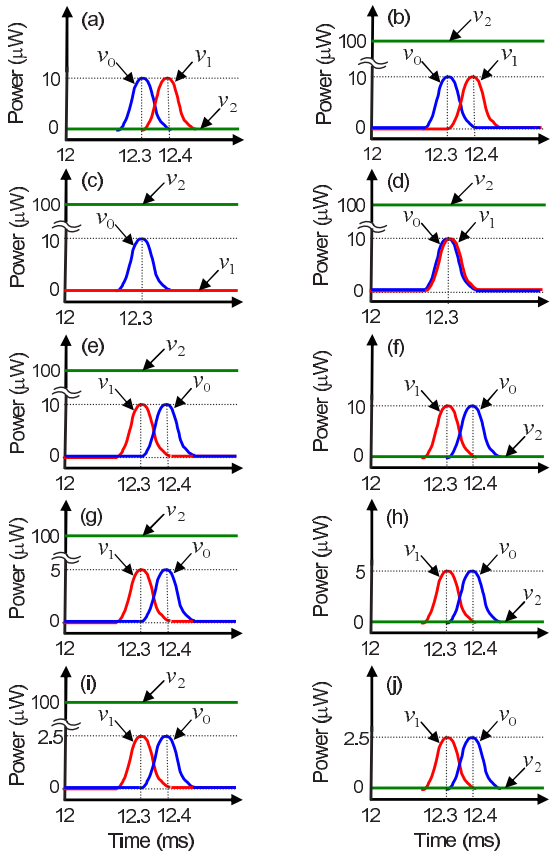

FIG. 6. (Color online) Intensities of the fields for population transfer in step 2 in the present experiment. The origin of time corresponds to that in Fig. 4.

ferent transition dipole moments contribute to the absorption of the probe in the present experiment, because we treat three types of ions shown in Fig. 5 simultaneously. Therefore, the estimation of the population is more difficult. However, it is shown here and in Appendix A that the average population of $|1\rangle$ of type-I and type-II ions can be approximately estimated from the measured transmittance of the probe.

The transmittance, $T_p(t)$, of the probe can be calculated by solving the following equations [30,80]:

$$\frac{\partial}{\partial t}\rho^{(J)}(t,z,\Delta) = -\frac{i}{\hbar}[H(t,z,\Delta,\mu_J),\rho^{(J)}(t,z,\Delta)] + L[\rho^{(J)}(t,z,\Delta)], \tag{17}$$

$$\frac{\partial}{\partial z}E_p(t,z) = i\hbar NC\sum_{J=\mathrm{I,II,III}}\mu_J\int\rho_{e,1}^{(J)}(t,z,\Delta)P_J(\Delta)d\Delta, \tag{18}$$

with

$$\rho^{(J)}(t,z,\Delta) = \sum_{k,l=1,e}\rho_{k,l}^{(J)}(t,z,\Delta)|k\rangle\langle l| = \begin{pmatrix}\rho_{1,1}^{(J)}(t,z,\Delta) & \rho_{1,e}^{(J)}(t,z,\Delta)\\ \rho_{e,1}^{(J)}(t,z,\Delta) & \rho_{e,e}^{(J)}(t,z,\Delta)\end{pmatrix}, \tag{19}$$

$$H(t,z,\Delta,\mu_J) = \hbar\,\Delta|e\rangle\langle e| + i\mu_J[E_p(t,z)|e\rangle\langle 1| - E_p^*(t,z)|1\rangle\langle e|], \tag{20}$$

$$L[\rho^{(J)}(t,z,\Delta)] = \begin{pmatrix}p_1\gamma\rho_{e,e}^{(J)}(t,z,\Delta) & -\gamma_p\rho_{1,e}^{(J)}(t,z,\Delta)\\ -\gamma_p\rho_{e,1}^{(J)}(t,z,\Delta) & -\gamma\rho_{e,e}^{(J)}(t,z,\Delta)\end{pmatrix}, \tag{21}$$

$$C = \frac{2\pi}{\hbar\epsilon_0 n\lambda}, \tag{22}$$

$$\rho^{(J)}(0,z,\Delta) = \begin{pmatrix}1 & 0\\ 0 & 0\end{pmatrix}, \tag{23}$$

$$E_p(t,0) = E_p^{(0)}. \tag{24}$$

Here, J represents the ionic type (I, II, or III); the z axis is set along the direction of the light beam; $\rho^{(J)}(t,z,\Delta)$ is the density matrix describing the states of the type-J ions with detuning Δ and at position z; $E_p(t,z)$ is the electric field of the probe at z; μ_J is the transition dipole moment of the $|1\rangle$-$|e\rangle$ transition of type-J ions; N is the ionic density per unit volume per unit detuning frequency; $P_J(\Delta)$ is the population distribution of $|1\rangle$ of type-J ions with respect to Δ just before the probe is injected; γ and γ_p are the population dumping rate and the dephasing rate for optical transitions, respectively; p_1 is the probability that the ions decay from $|e\rangle$ to $|1\rangle$ (for simplicity, p_1 is assumed to be independent of the ionic type); ϵ_0 is the permittivity of vacuum; n is the refractive index of the YSO crystal; λ is the laser wavelength; $E_p^{(0)}$ is the electric field corresponding to the constant incident intensity of the probe. In the present experiment, $\lambda = 606$ nm and $n = 1.8$ [81]. $T_p(t)$ is given by $|E_p(t,l)|^2/|E_p^{(0)}|^2$, where l is the crystal length (3 mm).

As shown in Appendix A, some approximations allow one to calculate $T_p(t)$ by the following simpler equations:

$$\frac{\partial}{\partial t}\bar{\rho}(t,z,\Delta) = -\frac{i}{\hbar}[H(t,z,\Delta,\bar{\mu}),\bar{\rho}(t,z,\Delta)] + L[\bar{\rho}(t,z,\Delta)], \tag{25}$$

$$\frac{\partial}{\partial z}\bar{\Omega}_p(t,z) = i\mu_s^2 NC\int\bar{\rho}_{e,1}(t,z,\Delta)\bar{P}(\Delta)d\Delta, \tag{26}$$

where $\mu_s^2 \equiv \mu_I^2 + \mu_{II}^2$, $\bar{\rho}(t,z,\Delta)$ denotes an average density matrix, $\bar{\mu}$ denotes an average transition dipole moment, $\bar{\Omega}_p(t,z) \equiv \bar{\mu}E_p(t,z)/\hbar$, and $\bar{P}(\Delta)$ denotes the average population distribution of type-I and type-II ions defined as

$$\bar{P}(\Delta) = \frac{\mu_\mathrm{I}^2 P_\mathrm{I}(\Delta) + \mu_\mathrm{II}^2 P_\mathrm{II}(\Delta)}{\mu_\mathrm{I}^2 + \mu_\mathrm{II}^2} \tag{27}$$

(see Appendix A for details). It should be noted that Eqs. (25) and (26) are equivalent to those in the case where the probe interacts with only a single transition [30]. $T_p(t)$ is given by $|\bar{\Omega}_p(t,l)|^2/|\bar{\Omega}_p^{(0)}|^2$, where $\bar{\Omega}_p^{(0)} = \bar{\mu}E_p^{(0)}/\hbar$.

In this paper, we estimate the average population distribution, $\bar{P}(\Delta)$, of type-I and type-II ions by fitting a theoretical curve calculated with Eqs. (25) and (26) to measured data of $T_p(t)$ using the least squares method. By estimating $\bar{P}(\Delta)$, we can estimate the population of ions with a specific value of Δ, as mentioned in Sec. III C. The fitting parameters are $\bar{\Omega}_p^{(0)}$ and the parameters determining $\bar{P}(\Delta)$ [see Eqs. (28) and (29)]. The other parameters are set as follows: γ and γ_p are set to 6 kHz and 9 kHz, respectively [79]; μ_{I} and μ_{II} are set to 1.7×10^{-32} C m and 2.1×10^{-32} C m, respectively [77]; p_1 is set to 0.5, which is the average of the values for type-I and type-II ions determined by assuming that the probability is proportional to the oscillator strength [77]; N is set to 0.097 $\mu\mathrm{m}^{-3}$ kHz^{-1}, which were estimated in the same manner as Ref. [30]. The uncertainties with respect to the decay are unimportant since the data in short time (20 μs) are used for the estimation.

IV. RESULTS

We performed the experiments in which the intensities of the three fields in step 2 (see Fig. 4 and Sec. III D) were set as Fig. 6. It should be noted that the necessary condition for STIRAP that the initial state, $|0\rangle$, is a dark state is satisfied except for the case of Fig. 6(a). The results are shown in Figs. 7 and 8. Figure 7 shows the transmittance of the probe. The circles and the curves show the measured data and the theoretical fits, respectively. The data were accumulated over 64 cycles as mentioned in Sec. III A. To take the bandwidth of the SA into account, the calculated curves were averaged at each time over 1.2 μs on a linear scale. In addition, to take into account the jitter of the time at which the probe rises, the calculated curves were averaged at each time over 1.2 μs on a log scale. The origin of time was roughly set so that the intensity of the probe reaches the plateau at $t=0$. Figure 8 shows the average population distributions, $\bar{P}(\Delta)$, of $|1\rangle$ of type-I and type-II ions, which were estimated from the fitting. The fitting was performed as explained in Sec. III E. The function form of $\bar{P}(\Delta)$ in the cases of Figs. 6(b)–6(j) was assumed as follows:

$$\bar{P}(\Delta) = a_1 \frac{a_2^2}{\Delta^2 + a_2^2} + a_3. \tag{28}$$

In the case of Fig. 6(a), $\bar{P}(\Delta)$ was assumed as follows:

$$\bar{P}(\Delta) = a_1 \frac{a_2^2}{\Delta^2 + a_2^2} + a_3 - a_4 e^{-\Delta^2/a_5^2}. \tag{29}$$

The fitting parameters are the incident Rabi frequency, $\bar{\Omega}_p^{(0)}$, of the probe and the parameters, a_j $(j=1,\ldots,5)$, determining $\bar{P}(\Delta)$.

The maximum Rabi frequency corresponding to the $|^3H_4, \pm 1/2\rangle$-$|^1D_2, \pm 1/2\rangle$ transition was also estimated in the same manner as Ref. [30], where the maximum intensity of the field of frequency ν_0 was set to about 10 μW. From this estimation and the transition dipole moments reported in Ref. [77], the maximum Rabi frequencies, $\Omega_j^{(0)}/2\pi$ $(j=0,1,2)$, in the case of Fig. 6(b) were estimated as shown in Table I. The adiabatic condition for the ideal tripod STIRAP process, $T_0 \gg \Omega_2^{(0)-1}$ and $T_1 \gg \Omega_2^{(0)-1}$, is satisfied for type-I and type-II ions.

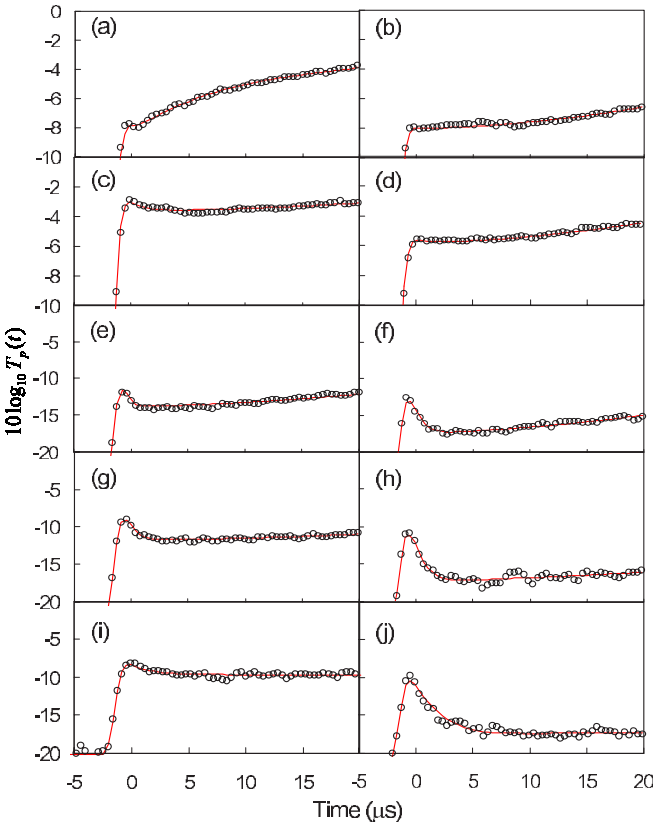

FIG. 7. (Color online) Measured transmittance, $T_p(t)$, of the probe. The circles and the curves show the measured data and the theoretical fits, respectively. Figures (a)–(j) correspond to Figs. 6(a)–6(j), respectively. The origin of time is roughly set so that the intensity of the probe reaches the plateau at $t=0$.

V. DISCUSSION

A natural question is whether or not the process inducing the observed population transfers was a coherent process, especially STIRAP. In this section, we first qualitatively discuss whether the observed population transfers were due to optical pumping or not, and confirm that the experimental results are consistent with the expectation based on the theory for STIRAP presented in Sec. II. Next, using numerical simulation, we discuss whether the observed population transfers were due to the STIRAP process or not. Finally, we present the estimation of the achieved fidelity as a one-qubit gate using the simulation. (As mentioned in Sec. II, the coherent population transfer via tripod STIRAP can be used as a one-qubit gate.)

A. Qualitative discussion

We first compare and discuss the cases of Figs. 6(a) and 6(b). The difference between these cases is only the absence

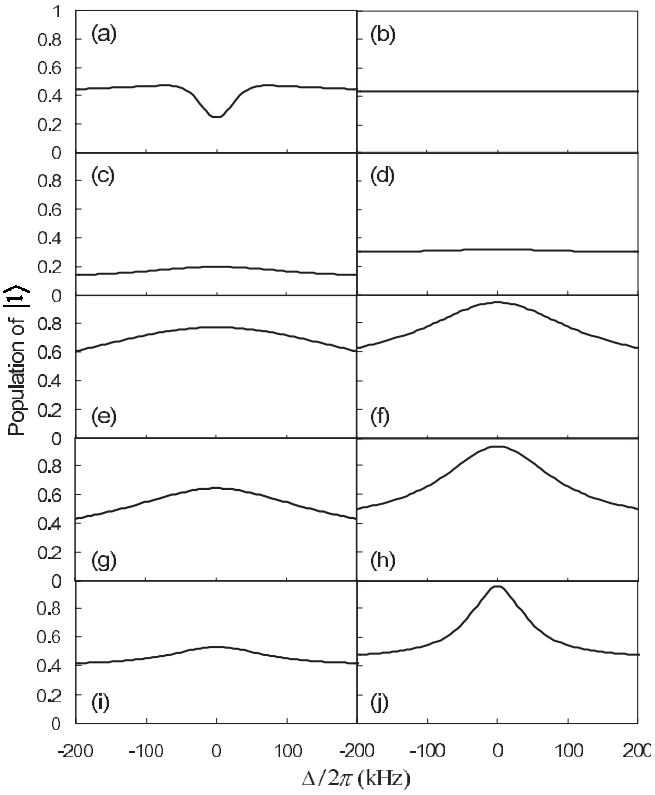

FIG. 8. Average population distribution, $\bar{P}(\Delta)$, of $|1\rangle$ of type-I and type-II ions, which was estimated from the fitting shown in Fig. 7. Figures (a)–(j) correspond to Figs. 6(a)–6(j), respectively.

of the field of frequency ν_2 in step 2 in the case of Fig. 6(a). In these cases, the order of the pulse sequence is "intuitive." As shown in Fig. 8(a), the transferred population distribution in the case of Fig. 6(a) has a dip at $\Delta=0$. The reason for the dip is physically explained as follows [30]. In the case of Fig. 6(a), where the necessary condition for STIRAP is not satisfied as mentioned in Sec. IV, the population of the ions with small detuning are transferred from $|0\rangle$ to $|1\rangle$ by optical pumping. The population transfer due to the optical pumping is not efficient, since the pulse resonating with the $|1\rangle$-$|e\rangle$ transition, which reduces the population of $|1\rangle$ by optical pumping, comes after the pulse resonating with the $|0\rangle$-$|e\rangle$ transition, which induces the population transfer from $|0\rangle$ to $|1\rangle$. On the other hand, the population of the ions with relatively large detuning is transferred by a coherent process such as off-resonant Raman transition. Consequently, the transferred population distribution in the case of Fig. 6(a) has a dip at $\Delta=0$. In contrast, in the case of Fig. 6(b), it is expected that the population is transferred via a tripod STIRAP process as explained in Sec. II. As shown in Fig. 8(b), the transferred population distribution in the case of Fig. 6(b) is almost constant with respect to Δ, and is larger than that in the case of Fig. 6(a) around $\Delta=0$. This result indicates that the population transfer around $\Delta=0$ in the case of Fig. 6(b) was mainly due not to optical pumping but the tripod STIRAP process, as expected.

Second, we compare the cases of Figs. 6(b) and 6(c). The difference between these cases is only the absence of the pulse of frequency ν_1 in step 2 in the case of Fig. 6(c). The transferred population in the case of Fig. 6(c) is smaller than that in the case of Fig. 6(b), as shown in Figs. 8(b) and 8(c). It may be difficult to explain this result only by optical pumping, because the optical pumping by the pulse of ν_1 in the case of Fig. 6(b) reduces the population of $|1\rangle$ and leads to the smaller population of $|1\rangle$ than in the case of Fig. 6(c). On the other hand, this experimental result is consistent with the expectation based on the geometric phase [from Eqs. (7), (8), and (15), $\Theta=0$ in the case of Fig. 6(c)]. Thus this result indicates that STIRAP had a large effect on the population transfers in these cases.

Next, we compare the cases of Figs. 6(b) and 6(d). The difference between these cases is only the delay time of the pulse sequence: $T_d=-T$ and $T_d=0$ in the cases of Figs. 6(b) and 6(d), respectively. The transferred population in the case of Fig. 6(d) is smaller than that in the case of Fig. 6(b), as shown in Figs. 8(b) and 8(d). This result is consistent with Fig. 2(a). However, the transferred population in the case of Fig. 6(d) is quite large compared with the value (zero) expected from Fig. 2(a). The reason for this discrepancy is discussed later with numerical simulation.

Finally, we discuss the cases of Figs. 6(e), 6(g), and 6(i). The difference among the three cases is only in the peak intensities of the pulses. In these cases, the order of the pulse sequence is "counterintuitive." As shown in Figs. 8(e), 8(g), and 8(i), the smaller intensities of the two pulses lead to smaller transferred population. It should be noted that this reduction of the transferred population is not due to the lack of the Rabi frequencies of the pulses, because efficient population transfers by Λ STIRAP were confirmed with the pulses of the same intensities, as shown in Figs. 8(f), 8(h), and 8(j). This intensity dependence is consistent with Fig. 2(b). The intensity-dependent reduction of the transferred population in the presence of the field of frequency ν_2 indicates that the tripod STIRAP process had a large effect on the population transfers in these cases.

B. Analysis with numerical simulation

Here, using numerical simulation, we discuss whether or not the process inducing the observed population transfers was a coherent process, especially the STIRAP process. We consider only the case where $\Delta=0$. The details of the numerical simulation used here is presented in Appendix B. This simulation well reproduces the experimental results, as shown in Fig. 12 [82].

The transferred population calculated by the geometric phase [Eq. (15)] with the Rabi frequencies used for the simulation is shown in Table II. The discrepancy between the calculated and experimental results is quite large. This means that the population transfers in the present experiment are not due to ideal STIRAP processes. This discrepancy is mainly due to two-photon detunings, because the calculated results by the geometric phase are in good agreement with those by the simulation without two-photon detunings, as shown in Table II. This also means that the effects of decoherences are small. Although the experimental results do not agree to the ideal case where the population is determined by the geometric phase, the experimental results indicate that the observed

TABLE II. Transferred population of the ions with zero one-photon detuning ($\Delta=0$). "Experiment" column shows the experimental results. "Geometric" column shows the population calculated using Θ defined by Eq. (15). "No detuning" column shows the population calculated by the simulation setting two-photon detunings to zero ($\delta_0=\delta_2=0$).

	Experiment	Geometric	No detuning
Fig. 6(b)	0.44	0.36	0.36
Fig. 6(c)	0.20	0	0.08
Fig. 6(d)	0.32	0.05	0.15
Fig. 6(e)	0.77	0.47	0.49
Fig. 6(g)	0.64	0.29	0.32
Fig. 6(i)	0.53	0.14	0.18

population transfers were due to not optical pumping but some coherent process similar to STIRAP, as discussed in Sec. V A. In the following, we discuss whether the process inducing the observed population transfers is similar to the STIRAP process or not.

Characteristic features of STIRAP are as follows [83].

(1) The excited state is almost unpopulated during the process, despite one-photon resonance.

(2) The effect of spontaneous emission is small, because of the first characteristic.

(3) The population transfer is a coherent process in the sense that the coherence among the ground states is necessary for the process.

In the following, using the numerical simulation, we show that the process inducing the observed population transfers has the above features of STIRAP.

First, we examine whether the excited state is unpopulated or not. Figure 9 shows the population of $|e\rangle$ estimated by the simulation, which was averaged with respect to the two-photon detunings, δ_0 and δ_2. The one-photon detuning, Δ, is set as $\Delta=0$. As expected, the excited-state populations in the cases of Figs. 6(b)–6(j) are small compared with that in the case of Fig. 6(a).

Next, we estimate how much population was transferred via optical pumping, to examine whether the effect of spontaneous emission is small or not. Here, the population transfer via optical pumping means that the population is transferred by the decay from $|e\rangle$ to ground states. This estimation can be easily achieved by using modified quantum trajectory simulation explained in Appendix C. The result is summarized in Table III. From Table III, it turns out that the probability of spontaneous emission is low except for the case of Fig. 6(a), as expected. Moreover, Table III also shows that most population is transferred by some process other than optical pumping except for the cases of Figs. 6(a) and 6(c) [84]. These results show that the effect of spontaneous emission is small in the cases of Figs. 6(b)–6(j).

Finally, we discuss whether the coherence among the ground states is necessary for the observed population transfers. Figure 10 shows the calculation result of the dependence of the transferred population on the dephasing rate, γ'_p,

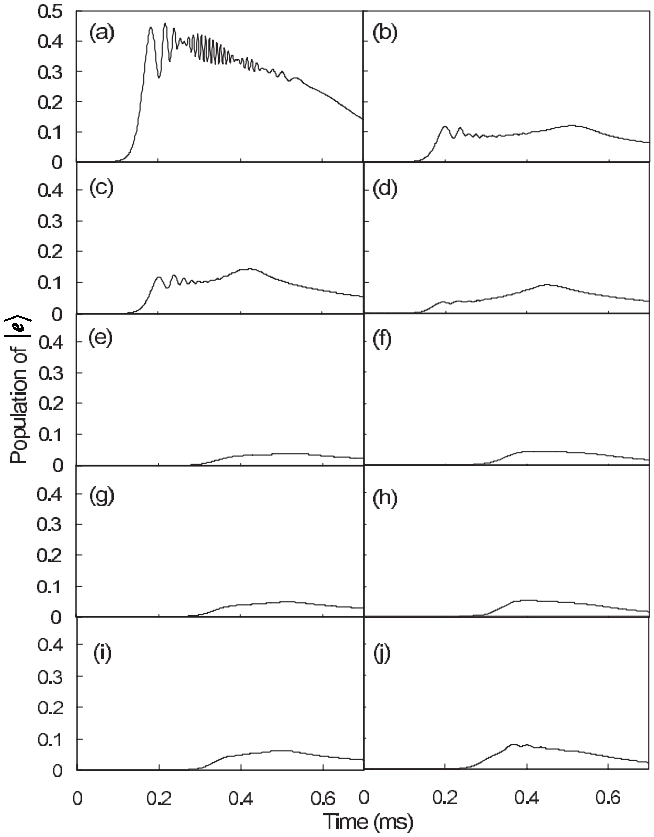

FIG. 9. Population of $|e\rangle$ during the population transfer estimated by the simulation, which was averaged with respect to the two-photon detunings, δ_0 and δ_2. The one-photon detuning, Δ, is set as $\Delta=0$. The origin of time is set to the time at which step 2 (population transfer) starts. Figures (a)–(j) correspond to Figs. 6(a)–6(j), respectively.

for hyperfine transitions. The circles, triangles, and squares in Fig. 10(a) correspond to Figs. 6(b), 6(c), and 6(d), respectively. The circles, triangles, and squares in Fig. 10(b) correspond to Figs. 6(e), 6(g), and 6(i), respectively. Figure 10(a) shows that the absence of the coherence among the ground states makes the transferred population in the case of Fig. 6(b) smaller than those in the cases of Figs. 6(c) and 6(d), which obviously contradicts the experimental results. On the other hand, Fig. 10(b) shows that the absence of the coherence among the ground states makes the transferred populations in the cases of Figs. 6(e), 6(g), and 6(i) smaller and equal to one another, which also contradicts the experimental results. Therefore, it is concluded that the coherence among the ground states is necessary for the population transfers in the present experiment.

Thus it turns out that the process inducing the population transfers in the present experiment is similar to STIRAP in the sense that this process possesses the characteristic features of STIRAP. It should be noted that even in the case of "intuitive" pulse sequence the population transfer is mainly due to the coherent process because of the presence of the third field. This is significant since this is the very characteristic of tripod STIRAP required to realize single-qubit rotations.

TABLE III. Estimation of the transferred population via optical pumping. The one-photon detuning, Δ, is set to zero. The "Total" column shows the simulation results of the transferred population shown in Fig. 12. The "Via optical pumping" column shows the transferred population via optical pumping estimated by the modified quantum trajectory simulation. The "Without decay" column shows the transferred population via the process other than optical pumping estimated by the modified quantum trajectory simulation. The ratios in the parentheses are those to the total transferred populations. The "Decay probability" column shows the probability of spontaneous emission during the population transfer estimated by the modified quantum trajectory simulation.

	Total	Via optical pumping	Without decay	Decay probability
Fig. 6(a)	0.31	0.18 (59%)	0.13 (41%)	0.72
Fig. 6(b)	0.45	0.09 (20%)	0.36 (80%)	0.25
Fig. 6(c)	0.17	0.17 (100%)	0 (0%)	0.28
Fig. 6(d)	0.29	0.08 (28%)	0.21 (72%)	0.16
Fig. 6(e)	0.76	0.04 (6%)	0.71 (94%)	0.06
Fig. 6(f)	0.93	0.04 (4%)	0.89 (96%)	0.07
Fig. 6(g)	0.66	0.06 (8%)	0.61 (92%)	0.08
Fig. 6(h)	0.92	0.05 (5%)	0.87 (95%)	0.08
Fig. 6(i)	0.53	0.07 (13%)	0.46 (87%)	0.10
Fig. 6(j)	0.90	0.06 (7%)	0.84 (93%)	0.11

As mentioned in Sec. V A, the discrepancy between the experimental result and the theoretical prediction is quite large in the case of Fig. 6(d). The reason for this may come from the following: There are two-photon detunings in the experiment, which is not considered in the ideal case [Fig. 2(a)]; the delay time of the pulse sequence in the case of Fig. 6(d) is not exactly zero in the experiment because of the group-velocity reduction due to the dispersion of Pr:YSO (see Appendix B and Table V); and the resultant order of the pulse sequence is "counterintuitive" (see Table V) [85]. Consequently, the transferred population in the case of Fig. 6(d) becomes large compared with the value (zero) expected from the calculation in the ideal case [Fig. 2(a)].

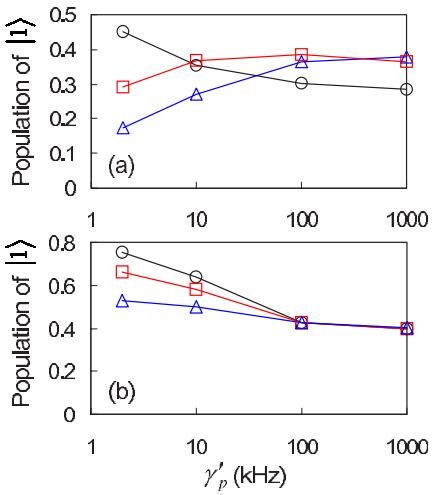

FIG. 10. (Color online) Dependence of transferred population on the dephasing rate, γ'_p (log scale), for hyperfine transitions, which was calculated by the simulation. (a) Circles, triangles, and squares correspond to Figs. 6(b), 6(c), and 6(d), respectively. (b) Circles, triangles, and squares correspond to Figs. 6(e), 6(g), and 6(i), respectively. The one-photon detuning, Δ, is set as Δ=0.

C. Fidelity as a one-qubit gate

As mentioned in Sec. II, tripod STIRAP can be used for not only coherent population transfer but also one-qubit gates. Here, we estimate the achieved fidelities in our experiment. We consider only a single ion with no detunings ($\Delta=\delta_0=\delta_2=0$) in which a qubit is stored [86,87]. The fidelity, F, is defined as follows:

$$F \equiv \langle\psi|\rho(t_f)|\psi\rangle, \tag{30}$$

where the ideal output state $|\psi\rangle$ is given by Eq. (16) and $\rho(t_f)$ is given by the numerical simulation used in the above discussion setting the detunings as $\Delta=\delta_0=\delta_2=0$ (t_f is the time at which the process finishes). The result is summarized in Table IV. As shown in Table IV, the fidelities are not very high. The dephasing between the hyperfine states is a main cause of the low fidelities. This turns out from the fact that the values of F' in Table IV are nearly equal to unity, where the values of F' are obtained by the numerical simulation assuming slower dephasing between the hyperfine states ($\gamma'_p=0.01$ kHz). It is known that this value of the dephasing

TABLE IV. Estimation of fidelities as one-qubit gates for the type-I and type-II ions with no detunings in the cases of Figs. 6(a) and 6(e). F is obtained by Eq. (30), where the ideal state $|\psi\rangle$ is given by Eq. (16) and ρ is given by the numerical simulation setting the detunings as $\Delta=\delta_0=\delta_2=0$. On the other hand, F' is obtained by the numerical simulation assuming slower dephasing between the hyperfine states ($\gamma'_p=0.01$ kHz).

	F	F'
Fig. 6(a) (Type I)	0.70	0.98
Fig. 6(a) (Type II)	0.67	0.99
Fig. 6(e) (Type I)	0.72	1.00
Fig. 6(e) (Type II)	0.68	0.94

rate can be achieved by an external magnetic field [57,58]. The application of an external field provides a further merit. By applying an external magnetic field, it may become possible to prepare the ionic state by optical pumping so that the two-photon detuning is ignored, since the ground states are split into six states by the Zeeman effect [88]. Thus it is expected that by applying an external magnetic field we may be able to realize higher fidelities as one-qubit gates and obtain them directly from experimental results.

VI. CONCLUSION

We have experimentally investigated a laser-driven four-level system in a tripod configuration in terms of stimulated Raman adiabatic passage (STIRAP) with a rare-earth-metal-ion-doped crystal ($Pr^{3+}:Y_2SiO_5$). The transferred population has been estimated from the measured transmittance of a weak probe. The experimental results indicate that the observed population transfers are mainly due to the process similar to STIRAP other than optical pumping. Using numerical simulation well reproducing the experimental results, we have discussed whether the process inducing the population transfers in the present experiment is the STIRAP process or not. The transferred populations observed in the present experiment are largely different from those calculated in the ideal case where the transferred populations are given by geometric phases. However, it has turned out that the process inducing the observed population transfers is a coherent process similar to STIRAP in the sense that this process possesses the following characteristic features of STIRAP: The excited state is almost unpopulated despite one-photon resonance; the effect of spontaneous emission is small; and the coherence among the ground states is necessary for the process. It is significant that even in the case of the "intuitive" pulse sequence the population transfer is mainly due to the coherent process because of the presence of the third field, because this is the very characteristic of tripod STIRAP which enables tripod STIRAP to realize single-qubit rotations. Thus, it is expected that the present experimental scheme can be directly applied to single-qubit rotations on a qubit stored in the hyperfine states of a rare-earth ion.

APPENDIX A: APPROXIMATION FOR THE ESTIMATION OF THE POPULATION DISTRIBUTION

Here we show that Eqs. (25) and (26) can be used for the fitting of a theoretical curve to the measured transmittance of the probe, instead of Eqs. (17) and (18). As a result, from the fitting, we can estimate the average population distribution, $\bar{P}(\Delta)$, of $|1\rangle$ of type-I and type-II ions, which is defined as Eq. (27).

First, the term proportional to μ_{III} in Eq. (18) is neglected because μ_{III} is much smaller than μ_{I} and μ_{II} ($\mu_{\mathrm{I}}=1.7\times10^{-32}$ C m, $\mu_{\mathrm{I}}=2.1\times10^{-32}$ C m, and $\mu_{\mathrm{I}}\leq0.3\times10^{-32}$ C m from Ref. [77]). Next, we assume that $P_{\mathrm{I}}(\Delta)$ is approximately proportional to $P_{\mathrm{II}}(\Delta)$ and they can be expressed as $P_J(\Delta)=P_J^{(0)}g(\Delta)+\delta P_J(\Delta)$ ($J=\mathrm{I},\mathrm{II}$), where $P_{\mathrm{I}}^{(0)}$ and $P_{\mathrm{II}}^{(0)}$ are positive constants, $g(\Delta)$ is a positive function, and $|\delta P_J(\Delta)|\ll P_J^{(0)}g(\Delta)$. Notice that this assumption includes the case where $P_{\mathrm{I}}(\Delta)\simeq P_{\mathrm{II}}(\Delta)$. Finally, regarding $E_p(t,z)$ in Eq. (17) as a given function, we express $\rho_{e,1}^{(J)}(t,z,\Delta)$ as $\mu_J E_p(t,z)f(t,z,\Delta,\mu_J)$, and approximate f to the first order of $\delta\mu_J\equiv\mu_J-\bar{\mu}$ ($J=\mathrm{I},\mathrm{II}$), where $\bar{\mu}$ is the average dipole moment defined as

$$\bar{\mu}=\frac{\mu_{\mathrm{I}}^3P_{\mathrm{I}}^{(0)}+\mu_{\mathrm{II}}^3P_{\mathrm{II}}^{(0)}}{\mu_{\mathrm{I}}^2P_{\mathrm{I}}^{(0)}+\mu_{\mathrm{II}}^2P_{\mathrm{II}}^{(0)}}. \tag{A1}$$

Then, $f(t,z,\Delta,\mu_J)$ becomes

$$f(t,z,\Delta,\mu_J)=f^{(0)}(t,z,\Delta)+f^{(1)}(t,z,\Delta)\delta\mu_J, \tag{A2}$$

with

$$f^{(0)}(t,z,\Delta)\equiv f(t,z,\Delta,\bar{\mu}), \tag{A3}$$

$$f^{(1)}(t,z,\Delta)\equiv \left.\frac{\partial}{\partial\mu_J}f(t,z,\Delta,\mu_J)\right|_{\mu_J=\bar{\mu}}. \tag{A4}$$

Then, we obtain

$$\frac{\partial}{\partial z}\bar{\Omega}_p(t,z)\simeq i\hbar NC\mu_s^2\bar{\Omega}_p(t,z)\int f^{(0)}(t,z,\Delta)\bar{P}(\Delta)d\Delta$$

$$=i\mu_s^2NC\int\bar{\rho}_{e,1}(t,z,\Delta)\bar{P}(\Delta)d\Delta, \tag{A5}$$

with

$$\bar{\Omega}_p(t,z)\equiv\frac{\bar{\mu}E_p(t,z)}{\hbar}, \tag{A6}$$

$$\mu_s^2\equiv\mu_{\mathrm{I}}^2+\mu_{\mathrm{II}}^2, \tag{A7}$$

$$\bar{\rho}_{e,1}(t,z,\Delta)\equiv\hbar\,\bar{\Omega}_p(t,z)f^{(0)}(t,z,\Delta)$$

$$=\bar{\mu}E_p(t,z)f(t,z,\Delta,\bar{\mu}). \tag{A8}$$

$\bar{\rho}_{e,1}$ is the element of the density matrix determined by the master equation (25). The transmittance, $T_p(t)$, of the probe is given by $|E_p(t,l)|^2/|E_p^{(0)}|^2=|\bar{\Omega}_p(t,l)|^2/|\bar{\Omega}_p^{(0)}|^2$. Thus, it turns out that we can use Eqs. (25) and (26) to calculate $T_p(t)$, instead of Eqs. (17) and (18).

Numerical calculation also supports the validity of the above approximation. We calculated $T_p(t)$ by numerical calculation with Eqs. (17) and (18), and fitted a theoretical curve calculated with Eqs. (25) and (26) to the calculated $T_p(t)$. In calculating $T_p(t)$ with Eqs. (17) and (18), the population distributions for three types of ions were assumed as follows:

$$P_{\mathrm{I}}(\Delta)=0.5+X, \tag{A9}$$

$$P_{\mathrm{II}}(\Delta)=0.5-X, \tag{A10}$$

$$P_{\mathrm{III}}(\Delta)=0\text{ or }1, \tag{A11}$$

and the other parameters were set to the values used for the fitting in Fig. 7. The result of the estimation of $\bar{P}$ from the

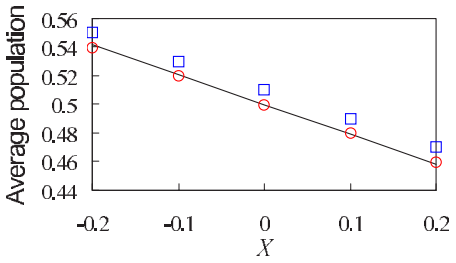

FIG. 11. (Color online) Calculated average population distribution, $\bar{P}$, of $|1\rangle$ of type-I and type-II ions when the population distributions for three types of ions are set as Eqs. (A9)–(A11). The solid line shows $\bar{P}$ obtained from the definition (27) and Eqs. (A9) and (A10). The circles and the squares show $\bar{P}$ estimated by fitting a theoretical curve calculated with Eqs. (25) and (26) to the calculated transmittance with Eqs. (17) and (18). The circles and the squares correspond to the cases where $P_{\mathrm{III}}(\Delta)=0$ and $P_{\mathrm{III}}(\Delta)=1$, respectively. It has been assumed in the estimation that $\bar{P}$ is constant with respect to Δ.

fitting is shown in Fig. 11, where $\bar{P}$ has been assumed to be constant with respect to Δ. The solid line shows $\bar{P}$ obtained from the definition (27) and Eqs. (A9) and (A10). On the other hand, the circles and the squares in Fig. 11 show $\bar{P}$ estimated by the above fitting in the cases where $P_{\mathrm{III}}(\Delta)=0$ and $P_{\mathrm{III}}(\Delta)=1$, respectively. Figure 11 shows that the estimation of $\bar{P}$ using Eqs. (25) and (26) is fairly good.

APPENDIX B: NUMERICAL SIMULATION

We performed numerical simulation of the population transfer in the tripod system for the discussion presented in Sec. V. Here we describe in detail how the simulation was performed.

We solve numerically the follow master equation for a four-level tripod system:

$$\frac{d}{dt}\rho(t,\Delta,\delta_0,\delta_2) = -\frac{i}{\hbar}[H(t),\rho(t,\Delta,\delta_0,\delta_2)] + L[\rho(t,\Delta,\delta_0,\delta_2)], \tag{B1}$$

where $H(t)$ is the Hamiltonian given by Eq. (1) and

$$\rho = \sum_{k,l=0,1,2,e} \rho_{k,l}|k\rangle\langle l| = \begin{pmatrix} \rho_{0,0} & \rho_{0,1} & \rho_{0,2} & \rho_{0,e} \\ \rho_{1,0} & \rho_{1,1} & \rho_{1,2} & \rho_{1,e} \\ \rho_{2,0} & \rho_{2,1} & \rho_{2,2} & \rho_{2,e} \\ \rho_{e,0} & \rho_{e,1} & \rho_{e,2} & \rho_{e,e} \end{pmatrix}, \tag{B2}$$

$$L[\rho] = \begin{pmatrix} p_0\gamma\rho_{e,e} & -\gamma_p'\rho_{0,1} & -\gamma_p'\rho_{0,2} & -\gamma_p\rho_{0,e} \\ -\gamma_p'\rho_{1,0} & p_1\gamma\rho_{e,e} & -\gamma_p'\rho_{1,2} & -\gamma_p\rho_{1,e} \\ -\gamma_p'\rho_{2,0} & -\gamma_p'\rho_{2,1} & p_2\gamma\rho_{e,e} & -\gamma_p\rho_{2,e} \\ -\gamma_p\rho_{e,0} & -\gamma_p\rho_{e,1} & -\gamma_p\rho_{e,2} & -\gamma\rho_{e,e} \end{pmatrix}, \tag{B3}$$

$$\rho(0,\Delta,\delta_0,\delta_2) = \begin{pmatrix} 1 & 0 & 0 & 0 \\ 0 & 0 & 0 & 0 \\ 0 & 0 & 0 & 0 \\ 0 & 0 & 0 & 0 \end{pmatrix}. \tag{B4}$$

Here Δ is the one-photon detuning from the $|1\rangle$-$|e\rangle$ transition; δ_j $(j=0,2)$ is the two-photon detuning from the $|j\rangle$-$|1\rangle$ transition; γ and γ_p are the population dumping rate and the dephasing rate of optical transitions, respectively; γ_p' is the dephasing rates of hyper transitions; and p_j $(j=0,1,2)$ is the probability that the ions decay from $|e\rangle$ to $|j\rangle$. The parameters were set as follows: $\gamma=6$ kHz and $\gamma_p=9$ kHz [79]; $\gamma_p'=2$ kHz [56]; p_0, p_1, and p_2, were determined by assuming that the probability is proportional to the oscillator strength [77]. The Rabi frequencies were set as Table V. $\Omega_j^{(0)}$ $(j=0,1,2)$ in Table V were determined from Table I [89]. Since the transferred population is a little sensitive to the widths and the peak positions of the pulses, T_j and t_j $(j=0,1)$ in Table V were determined from the measured intensities of the pulses. The origin of time corresponds to that in Fig. 4. The cause of the larger values of T_1 in the cases of Figs. 6(a) and 6(b) than those in the other cases is probably stimulated Raman scattering. On the other hand, the cause of the delay of the pulse of frequency ν_0 is probably the group-velocity reduction due to the dispersion ofPr:YSO.

The calculation was performed from $t=12$ ms to $t_f=12.7$ ms. The calculation results are shown in Fig. 12. These are obtained by averaging $\rho_{1,1}(t_f,\Delta,\delta_0,\delta_2)$ with respect to δ_0 and δ_2. The two-photon-detuning distributions, $W(\delta_0)$ and $W(\delta_2)$, of the ions, which are due to the inhomogeneous broadenings of the $|0\rangle$-$|1\rangle$ and $|1\rangle$-$|2\rangle$ transitions, respectively, have been assumed as follows [78]:

$$W_0(\delta_0) = \begin{cases} 1 & |\delta_0|/2\pi \le 15 \text{ kHz} \\ 0 & \text{otherwise}, \end{cases} \tag{B5}$$

$$W_2(\delta_2) = \begin{cases} 1 & |\delta_2|/2\pi \le 35 \text{ kHz} \\ 0 & \text{otherwise}. \end{cases} \tag{B6}$$

The calculation results shown in Fig. 12 are in fairly good agreement with the experimental ones shown in Fig. 8.

APPENDIX C: MODIFIED QUANTUM TRAJECTORY SIMULATION

To estimate how much population was transferred via optical pumping, we have used modified quantum trajectory simulation (see Refs. [80,90–93] for details of standard quantum trajectory simulation). Here, we explain the theoretical method.

The master equation (B1) for the density operator describing the four-level tripod system is expressed as

$$\frac{d}{dt}\rho = \mathcal{L}[\rho] + \mathcal{S}[\rho], \tag{C1}$$

TABLE V. Rabi frequencies used for the simulation. $\Omega_j^{(0)}$ $(j=0,1,2)$, T_j $(j=0,1)$, and t_j $(j=0,1)$ are defined as Eqs. (2)–(4). The origin of time corresponds to that in Fig. 4.

	Ionic type	$\Omega_0^{(0)}/2\pi$	$\Omega_1^{(0)}/2\pi$	$\Omega_2^{(0)}/2\pi$	T_0	T_1	t_0	t_1
Fig. 6(a)	Type I	94	80	0	100	120	12.31	12.39
	Type II	78	98	0	100	120	12.31	12.39
Fig. 6(b)	Type I	94	80	63	100	115	12.32	12.40
	Type II	78	98	40	100	115	12.32	12.40
Fig. 6(c)	Type I	94	0	63	100		12.32	
	Type II	78	0	40	100		12.32	
Fig. 6(d)	Type I	94	80	63	100	110	12.32	12.30
	Type II	78	98	40	100	110	12.32	12.30
Fig. 6(e)	Type I	94	80	63	100	110	12.42	12.30
	Type II	78	98	40	100	110	12.42	12.30
Fig. 6(f)	Type I	94	80	0	100	110	12.42	12.30
	Type II	78	98	0	100	110	12.42	12.30
Fig.6(g)	Type I	66	57	63	100	110	12.42	12.30
	Type II	55	69	40	100	110	12.42	12.30
Fig. 6(h)	Type I	66	57	0	100	110	12.42	12.30
	Type II	55	69	0	100	110	12.42	12.30
Fig. 6(i)	Type I	47	40	63	100	110	12.42	12.30
	Type II	39	49	40	100	110	12.42	12.30
Fig. 6(j)	Type I	47	40	0	100	110	12.42	12.30
	Type II	39	49	0	100	110	12.42	12.30

where the superoperators $\mathcal{L}$ and $\mathcal{S}$ are defined as

$$\mathcal{L}[\rho] = -\frac{i}{\hbar}[H,\rho] + L[\rho] - \mathcal{S}[\rho], \tag{C2}$$

$$\mathcal{S}[\rho] = \sum_{j=0,1,2} p_j \gamma |j\rangle\langle e|\rho|e\rangle\langle j|. \tag{C3}$$

$\mathcal{L}$ corresponds to the process without spontaneous emission. On the other hand, $\mathcal{S}$ corresponds to quantum jump from $|e\rangle$ to the ground states due to spontaneous emission. The formal solution for Eq. (C1) is expressed as

$$\rho(t) = \sum_{m=0}^{\infty} \int_0^t dt_m \int_0^{t_m} dt_{m-1} \cdots \int_0^{t_2} dt_1 \times e^{\mathcal{L}(t-t_m)} \mathcal{S} e^{\mathcal{L}(t_m - t_{m-1})} \mathcal{S} \cdots \mathcal{S} e^{\mathcal{L}t_1} \rho(0). \tag{C4}$$

The density operator describing the state satisfying the condition that spontaneous emission never occurs is given by $e^{\mathcal{L}t}\rho(0)/\mathrm{Tr}[e^{\mathcal{L}t}\rho(0)]$. The probability that spontaneous emission never occurs during the population transfer is also given by $\mathrm{Tr}[e^{\mathcal{L}t_f}\rho(0)]$, where t_f denotes the time at which the population transfer finishes. The transferred population under the condition that spontaneous emission never occurs during the population transfer can be obtained by $\langle 1|e^{\mathcal{L}t_f}\rho(0)|1\rangle$. $e^{\mathcal{L}t}\rho(0)$ can be easily calculated by the following equation:

$$\frac{d}{dt}\rho = \mathcal{L}[\rho]. \tag{C5}$$

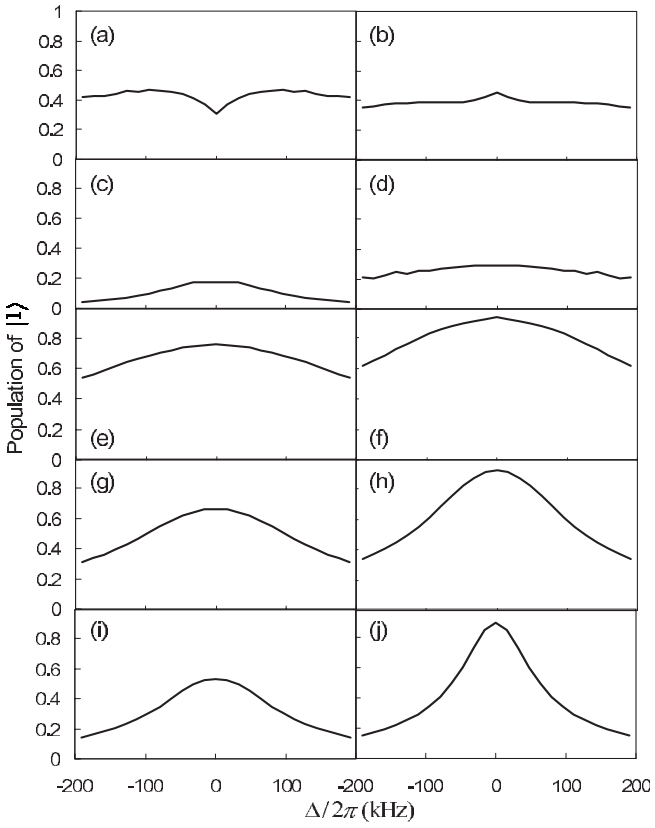

FIG. 12. Calculated average population distribution, $\bar{P}(\Delta)$, of $|1\rangle$ of type-I and type-II ions by the numerical simulation. Figures (a)–(j) correspond to Figs. 6(a)–6(j), respectively.

In standard quantum trajectory simulation, a Schrödinger equation with a non-Hermitian Hamiltonian is used instead of Eq. (C5), by using quantum-jump superoperators for all decoherences. In this sense, the present method is modified quantum trajectory simulation. The results shown in Table III are obtained in this manner.

[1] L. I. Schiff, *Quantum Mechanics* (McGraw-Hill, New York, 1955).
[2] A. Messiah, *Quantum Mechanics* (North-Holland, Amsterdam, 1962), Vol. 2.
[3] T. Pellizzari, S. A. Gardiner, J. I. Cirac, and P. Zoller, Phys. Rev. Lett. **75**, 3788 (1995).
[4] L.-M. Duan, J. I. Cirac, and P. Zoller, Science **292**, 1695 (2001).
[5] M. S. Shahriar *et al.*, Opt. Commun. **195**, 411 (2001).
[6] Z. Kis and F. Renzoni, Phys. Rev. A **65**, 032318 (2002).
[7] J. Pachos and H. Walther, Phys. Rev. Lett. **89**, 187903 (2002).
[8] H. Goto and K. Ichimura, Phys. Rev. A **70**, 012305 (2004).
[9] N. Sangouard, X. Lacour, S. Guérin, and H. R. Jauslin, Phys. Rev. A **72**, 062309 (2005).
[10] E. Arimondo, in *Progress in Optics*, edited by E. Wolf (Elsevier Science, Amsterdam, 1996), Vol. 35, p. 257.
[11] K. Bergmann, H. Theuer, and B. W. Shore, Rev. Mod. Phys. **70**, 1003 (1998).
[12] J. Oreg, F. T. Hioe, and J. H. Eberly, Phys. Rev. A **29**, 690 (1984).
[13] J. R. Kuklinski, U. Gaubatz, F. T. Hioe, and K. Bergmann, Phys. Rev. A **40**, 6741 (1989).
[14] B. W. Shore, J. Martin, M. P. Fewell, and K. Bergmann, Phys. Rev. A **52**, 566 (1995).
[15] J. Martin, B. W. Shore, and K. Bergmann, Phys. Rev. A **52**, 583 (1995).
[16] N. V. Vitanov and S. Stenholm, Phys. Rev. A **56**, 1463 (1997).
[17] N. V. Vitanov and S. Stenholm, Opt. Commun. **135**, 394 (1997).
[18] V. I. Romanenko and L. P. Yatsenko, Opt. Commun. **140**, 231 (1997).
[19] N. V. Vitanov, Phys. Rev. A **58**, 2295 (1998).
[20] G. G. Grigoryan and Y. T. Pashayan, Opt. Commun. **198**, 107 (2001).
[21] L. P. Yatsenko, V. I. Romanenko, B. W. Shore, and K. Bergmann, Phys. Rev. A **65**, 043409 (2002).
[22] Q. Shi and E. Geva, J. Chem. Phys. **119**, 11773 (2003).
[23] P. A. Ivanov, N. V. Vitanov, and K. Bergmann, Phys. Rev. A **70**, 063409 (2004).
[24] U. Gaubatz *et al.*, Chem. Phys. Lett. **149**, 463 (1988).
[25] U. Gaubatz, P. Rudechi, S. Schiemann, and K. Bergmann, J. Chem. Phys. **92**, 5363 (1990).
[26] P. Pillet, C. Valentin, R.-L. Yuan, and J. Yu, Phys. Rev. A **48**, 845 (1993).
[27] T. Halfmann and K. Bergmann, J. Chem. Phys. **104**, 7068 (1996).
[28] J. Martin, B. W. Shore, and K. Bergmann, Phys. Rev. A **54**, 1556 (1996).
[29] T. Peters, L. P. Yatsenko, and T. Halfmann, Phys. Rev. Lett. **95**, 103601 (2005).
[30] H. Goto and K. Ichimura, Phys. Rev. A **74**, 053410 (2006).
[31] R. Unanyan, M. Fleischhauer, B. W. Shore, and K. Bergmann, Opt. Commun. **155**, 144 (1998).
[32] R. G. Unanyan, B. W. Shore, and K. Bergmann, Phys. Rev. A **59**, 2910 (1999).
[33] R. G. Unanyan and M. Fleischhauer, Phys. Rev. A **69**, 050302(R) (2004).
[34] R. G. Unanyan, M. E. Pietrzyk, B. W. Shore, and K. Bergmann, Phys. Rev. A **70**, 053404 (2004).
[35] J. Ruseckas, G. Juzeliūnas, P. Öhberg, and M. Fleischhauer, Phys. Rev. Lett. **95**, 010404 (2005).
[36] H. Theuer, R. G. Unanyan, C. Habscheid, K. Klein, and K. Bergmann, Opt. Express **4**, 77 (1999).
[37] F. Vewinger, M. Heinz, R. GarciaFernandez, N. V. Vitanov, and K. Bergmann, Phys. Rev. Lett. **91**, 213001 (2003).
[38] *Geometric Phases in Physics*, edited by A. Shapere and F. Wilczek (World Scientific, Singapore, 1989).
[39] M. V. Berry, Proc. R. Soc. London, Ser. A **392**, 45 (1984).
[40] B. Simon, Phys. Rev. Lett. **51**, 2167 (1983).
[41] F. Wilczek and A. Zee, Phys. Rev. Lett. **52**, 2111 (1984).
[42] P. Zanardi and M. Rasetti, Phys. Lett. A **264**, 94 (1999).
[43] J. Pachos, P. Zanardi, and M. Rasetti, Phys. Rev. A **61**, 010305(R) (1999).
[44] J. A. Jones, V. Vedral, A. Ekert, and G. Castagnoli, Nature (London) **403**, 869 (2000).
[45] A. Recati, T. Calarco, P. Zanardi, J. I. Cirac, and P. Zoller, Phys. Rev. A **66**, 032309 (2002).
[46] A. O. Niskanen, M. Nakahara, and M. M. Salomaa, Phys. Rev. A **67**, 012319 (2003).
[47] P. Solinas, P. Zanardi, N. Zanghì, and F. Rossi, Phys. Rev. B **67**, 121307(R) (2003).
[48] M. Tian, Z. W. Barber, J. A. Fischer, and Wm. Randall Babbitt, Phys. Rev. A **69**, 050301(R) (2004).
[49] I. Fuentes-Guridi, F. Girelli, and E. Livine, Phys. Rev. Lett. **94**, 020503 (2005).
[50] G. Florio, P. Facchi, R. Fazio, V. Giovannetti, and S. Pascazio, Phys. Rev. A **73**, 022327 (2006).
[51] R. M. Macfarlane and R. M. Shelby, in *Spectroscopy of Solids Containing Rare-Earth Ions*, edited by A. A. Kaplyanskii and R. M. Macfarlane (North-Holland, Amsterdam, 1987), Chap. 3.
[52] R. Yano, M. Mitsunaga, and N. Uesugi, Opt. Lett. **16**, 1884 (1991).
[53] R. W. Equall, Y. Sun, R. L. Cone, and R. M. Macfarlane, Phys. Rev. Lett. **72**, 2179 (1994).
[54] Y. Sun, C. W. Thiel, R. L. Cone, R. W. Equall, and R. L. Hutcheson, J. Lumin. **98**, 281 (2002).
[55] R. M. Macfarlane, J. Lumin. **100**, 1 (2002).
[56] B. S. Ham, M. S. Shahriar, M. K. Kim, and P. R. Hemmer, Opt. Lett. **22**, 1849 (1997).
[57] E. Fraval, M. J. Sellars, and J. J. Longdell, Phys. Rev. Lett. **92**, 077601 (2004).
[58] E. Fraval, M. J. Sellars, and J. J. Longdell, Phys. Rev. Lett. **95**, 030506 (2005).

[59] K. Ichimura, Opt. Commun. **196**, 119 (2001).
[60] N. Ohlsson, R. K. Mohan, and S. Kröll, Opt. Commun. **201**, 71 (2002).
[61] J. Wesenberg and K. Mølmer, Phys. Rev. A **68**, 012320 (2003).
[62] I. Roos and K. Mølmer, Phys. Rev. A **69**, 022321 (2004).
[63] Y.-F. Xiao, Z.-F. Han, Y. Yang, and G.-C. Guo, Phys. Lett. A **330**, 137 (2004).
[64] Y.-F. Xiao, X. M. Lin, J. Gao, Y. Yang, Z. F. Han, and G. C. Guo, Phys. Rev. A **70**, 042314 (2004).
[65] B. S. Ham, M. S. Shahriar, and P. R. Hemmer, Opt. Lett. **22**, 1138 (1997).
[66] B. S. Ham, P. R. Hemmer, and M. S. Shahriar, Opt. Commun. **144**, 227 (1997).
[67] K. Ichimura, K. Yamamoto, and N. Gemma, Phys. Rev. A **58**, 4116 (1998).
[68] A. V. Turukhin, V. S. Sudarshanam, M. S. Shahriar, J. A. Musser, B. S. Ham, and P. R. Hemmer, Phys. Rev. Lett. **88**, 023602 (2001).
[69] J. J. Longdell, E. Fraval, M. J. Sellars, and N. B. Manson, Phys. Rev. Lett. **95**, 063601 (2005).
[70] J. J. Longdell and M. J. Sellars, Phys. Rev. A **69**, 032307 (2004).
[71] J. J. Longdell, M. J. Sellars, and N. B. Manson, Phys. Rev. Lett. **93**, 130503 (2005).
[72] L. Rippe, M. Nilsson, S. Kröll, R. Klieber, and D. Suter, Phys. Rev. A **71**, 062328 (2005).
[73] B. S. Ham and P. R. Hemmer, Phys. Rev. Lett. **84**, 4080 (2000).
[74] B. S. Ham, Appl. Phys. Lett. **78**, 3382 (2001).
[75] Z. Wu and H. Yang, Phys. Rev. A **72**, 012114 (2005).
[76] R. W. P. Drever *et al.*, Appl. Phys. B: Photophys. Laser Chem. **31**, 97 (1983).
[77] M. Nilsson, L. Rippe, S. Kröll, R. Klieber, and D. Suter, Phys. Rev. B **70**, 214116 (2004).
[78] K. Holliday, M. Croci, E. Vauthey, and U. P. Wild, Phys. Rev. B **47**, 14741 (1993).
[79] R. W. Equall, R. L. Cone, and R. M. Macfarlane, Phys. Rev. B **52**, 3963 (1995).
[80] P. Meystre and M. Sargent III, *Elements of Quantum Optics* (Springer-Verlag, Berlin, 1999).
[81] F. R. Graf, A. Renn, G. Zumofen, and U. P. Wild, Phys. Rev. B **58**, 5462 (1998).
[82] The considerable discrepancy between Figs. 8 and 12 when Δ is large may be due to the inefficient pumping in step 1 (initialization process).
[83] These features are also those of off-resonant Raman transition except for one-photon resonance. One-photon resonance distinguishes STIRAP from off-resonant Raman transition.
[84] The reason why the population transfer in the case of Fig. 6(c) is only due to optical pumping is that there is no coherent process inducing the population transfer to $|1\rangle$ in this case because $\Omega_1(t)=0$.
[85] As found from the comparison between Figs. 8(b) and 8(e), the pulse sequence in the "counterintuitive" order leads to larger transferred population than in the "intuitive" order in the presence of two-photon detunings as in the present experiment.
[86] If a qubit is stored in a single ion, the detunings due to inhomogeneous broadening can be ignored.
[87] This is a theoretical work rather than an experimental one in the sense that the estimated fidelities are not obtained directly from the experimental results. However, the present experimental results are significant since these support the simple theoretical model used for the numerical simulation.
[88] The reason why this preparation of the ionic state is impossible in the present experiment is that the ground state is split into three states (in the present experiment, an external field was not applied) and the tripod system requires at least three ground states. If there are six ground states, it may be possible to prepare the ionic state by optical pumping so that the ensemble of the ions used for tripod STIRAP has almost no two-photon detunings.
[89] The values of $\Omega_2^{(0)}$ in Table V were set to $1/\sqrt{2}$ of the values in Table I to explain the experimental results, especially the cases of Figs. 6(e), 6(g), and 6(i).
[90] H. J. Carmichael, in *An Open Systems Approach to Quantum Optics*, edited by W. Beiglböck, Lecture Notes in Physics Vol. m18, (Springer-Verlag, Berlin, 1993).
[91] M. O. Scully and M. S. Zubairy, *Quantum Optics* (Cambridge University Press, Cambridge, UK, 1997).
[92] K. Mølmer, Y. Castin, and J. Dalibard, J. Opt. Soc. Am. B **10**, 524 (1993).
[93] M. B. Plenio and P. L. Knight, Rev. Mod. Phys. **70**, 101 (1998).